Heliyon 9 (2023) e16975

Contents lists available at ScienceDirect

Heliyon

journal homepage: www.cell.com/heliyon

Effect of different synthesis methodologies on the adsorption of iodine

Guowei Yuan [a], Yizhong Lu [b], Cheng Yang [a,*]

[a] School of Chemistry and Chemical Engineering, University of Jinan, Jinan, 250022, China
[b] School of Materials Science and Engineering, University of Jinan, Jinan, 250022, China

ARTICLE INFO

Keywords:
Cu_2O
Iodine ion adsorption
Dynamic chemical plating
Cu_2O deposition Rate
Cu/ag-MOR

ABSTRACT

Radioactive nuclides such as cesium, ruthenium, and iodine are difficult to remove in radioactive wastewater, which could be removed by coprecipitation of special chemical precipitants. In this study, dynamic Cu/Ag-mordenite (Cu/Ag-MOR) material was synthesized to be treated as the precipitant to selectively adsorb the iodine ion (I^-) through controlled chemisorption combined with physical adsorption. XRD, XPS, and FTIR characterization demonstrated the successful modification of the MOR carrier surface by Cu/Ag particles and the high selectivity of the active component Cu (I) on the dynamic Cu/Ag-MOR material. SEM, TEM, and BET methods were used to characterize the Cu/Ag-MOR material, demonstrating these results: the MOR carried a stable porous structure, which allowed the silver to be well dispersed on its surface. The silver improved the copper distribution by being well-coated by the copper species. Furthermore, the analysis of the factors influencing the chemical plating of copper showed that the pH, the concentration of EDTA-2Na and the temperature all influenced the deposition rate of Cu_2O. The activation energy for Cu_2O deposition in dynamic Cu/Ag-MOR was 20.31 kJ/mol. The highest removal of I^- in the presence of dynamic Cu/Ag-MOR could reach 99.1% in the adsorption tests. The adsorption kinetics was under a proposed second-order model, with chemisorption being the controlling step of the reaction. The adsorption/desorption experiments demonstrated the reusability of the nanosorbent. It was also demonstrated that dynamic Cu/Ag-MOR materials showed good applicability in complex situations where multiple pollutants co-exist.

1. Introduction

As a new era of clean and efficient high-quality energy, nuclear energy has increasingly played a pivotal role in alleviating the existing energy shortage and environmental pollution [1]. In addition, it can regulate the global energy structure allocation. However, while the nuclear power industry is booming, it generates much radioactive wastewater [2,3], which causes environmental pollution and damage to humanity health. How to effectively and adequately treat this radioactive wastewater greatly impacts human life, environmental protection, and even the further planning of the nuclear energy industry. ^{129}I is one of the main radionuclides that contaminate groundwater [4–6]. Due to its long half-life, high activity in geological formations, and its ability to enrich animals and vital human body organs, its radioactive hazards have received wide attention [7]. Radioactive iodine is a significant hazard to organisms and the environment that needs to be enriched. Therefore, while developing a new generation of nuclear power, research on

* Corresponding author.
E-mail address: chm_yangch@ujn.edu.cn (C. Yang).

https://doi.org/10.1016/j.heliyon.2023.e16975
Received 21 February 2023; Received in revised form 27 May 2023; Accepted 2 June 2023
Available online 3 June 2023

rapid and efficient treatment technologies for contaminated radioactive wastewater plays a critical role in treating radioactive contamination in nuclear power plants and their surrounding environment under accidental working conditions [2].

The main methods of radioactive wastewater treatment are adsorption [8–10], ion exchange [11,12], permeation membrane separation [13], and precipitation [14]. The precipitation method is the simplest and most effective for removing radioactive iodine nuclides. This method generates precipitation of compounds with small concentration products by solubility product theory. In previous reports, Bi^{3+} [3], Hg^{2+} [15], Ag^{+} [16–20], and Cu^{+} [21] based compounds were used as suitable adsorbents to combine with iodine compounds in water [22,23] to form precipitates, thus solidifying volatile types of iodine compounds (I^{-}, I_2, IO^{-}, IO_3^{-}, CH_3I). The mechanism of adsorption of monomeric iodine relies on hydrophobic interaction [24] and complexation. When activated carbon is used for the adsorption of iodine molecules and iodate, the activated carbon only uses the hydrophobic effect of its pore channels to adsorb iodine molecules. However, iodide ions do not appear to have hydrophobic interaction. Thus the adsorption of iodide ions is mainly manifested as electrostatic physisorption and chemisorption [25]. The Cu/Ag-mordenite (Cu/Ag-MOR) material developed in this project selectively adsorbs element I from water bodies through controlled chemisorption combined with physical adsorption. References to previous papers [26–28], a pseudo-second-order model was developed to perform a kinetic analysis of dynamic Cu/Ag-MOR materials.

Among them, MOR has a large specific surface area and thus generates large diffusion forces. The interior of MOR has many uniformly sized pores and channels, which are connected to each other and to the outside world by open channels. Under certain physico-chemical conditions, MOR has a precise and fixed diameter and thus produces a "molecular sieve" effect. This means that substances smaller than this diameter are adsorbed and substances larger than this diameter are excluded. This is the physical adsorption mechanism of MOR.

Chemisorption relies on the strong interaction between Cu^{+}, I^{-}, Ag^{+} and I^{-}, resulting in the generation of CuI and AgI, which solidify the I^{-} and adsorb the I^{-} onto the MOR skeleton. In addition, the force of the adsorbent with iodide ions is related to the softness of the acid and base. I^{-} and Cu^{+} are soft bases and soft acids, which are prone to strong affinity. Cu^{2+} is the boundary acid and has a weaker interaction with I^{-}.

This article used different preparation methods to prepare Cu/Ag-MOR, including dynamic chemical plating and static chemical plating. Cu/Ag-MOR synthesized by dynamic chemical plating was treated as the precipitant to remove the iodine ion (I^{-}), which has excellent adsorption performance in disposing of I^{-} contamination wastewater. Ag-MOR and Cu-MOR were also prepared as a comparison. For Cu/Ag-MOR, Ag improved copper dispersed well through being coated by the copper species well. In addition, Cu^{+} was the active site on the Cu/Ag-MOR that could remove the iodine ions through the formation of CuI. Dynamic Cu/Ag-MOR materials prepared by dynamic chemical plating possess more Cu (I) than the static method. The highest removal rate of I^{-} in the presence of dynamic Cu/Ag-MOR could reach up to 99.1%.

2. Experimental

2.1. Materials and reagents

$C_{10}H_{14}N_2Na_2O_8{\cdot}2H_2O$ and $C_6H_{12}O_6$ were purchased from Sinopharm Chemical Reagent Co., Ltd while $NH_3{\cdot}H_2O$ and KI were bought by Shanghai Aladin Biochemical Technology Co., Ltd. HCHO, C_5H_5N were bought by XILONG SCIENTIFIC while $C_6H_5Na_3O_7{\cdot}2H_2O$ was purchased from MACKLIN. $CuSO_4$ and Na_2CO_3 were bought by Tianjin Kemiou Chemical Reagent Co., Ltd while $AgNO_3$ was purchased from Tianjin Fengchuan Chemical Reagent Co., Ltd. NaOH was bought by DAMAO CHEMICAL REAGENT FACTORY. The reagents were used as received without extra treatment. Mordenite (MOR) was obtained from Yingkou Zhongbao Molecular Sieve Co., Ltd. KI solution were simulated as wastewater. Deionized water were used in all experiment process.

2.2. Preparation of adsorbents

2.2.1. Preparation of Ag-MOR

The Ag-MOR was prepared according to the previous report [29–31]. The mass ratio of silver nitrate, sodium citrate, and mordenite is 1:3.9:164. The mordenite was put into water to make the suspension, then configured the concentration of 0.17 mol/L silver nitrate and added to the suspension. The mixture was heated for 1.5 h [17,18,31] to reach boiling under stirring and refluxing. The container containing the silver nitrate is then washed with deionized water and added to the suspension. Sodium citrate was put into the continuous boiling suspension for 1.5 h to obtain mercerized mordenite gel. The mass ratio of sodium carbonate and silver nitrate is 0.3:1, while the mass ratio of glucose and silver nitrate equals 0.7:1. Configured 0.1 mol/L sodium carbonate to the prepared mercerized mordenite gel and added glucose to stir well, then put the gel under water bath heating at 80 °C. After 30 min, the mixture was filtered at the pressure of 2.5 KPa to obtain the filter cake that was washed 4 times. The Ag-MOR was synthesized by drying the filter cake at 140 °C for 3 h.

2.2.2. Preparation of cu/ag-MOR

2.2.2.1. Dynamic Cu/Ag-MOR. In this project, the parallel solution was introduced; it was prepared by dropping copper sulfate, pyridine, and ethylene diamine tetra acetic acid disodium salt (EDTA-2Na) to sodium hydroxide 3 h and stabilized for 2 h under a water heating bath at 70 °C. Dynamic chemical plating is a method of adding a parallel solution that droplets to the reducing agent,

including formaldehyde, sodium hydroxide, and Ag-MOR. The material synthesized by the dynamic chemical plating method was named dynamic Cu/Ag-MOR.

2.2.2.2. Static cu/ag-MOR. The static chemical plating of Cu/Ag-MOR was prepared according to the previous report [32,33]. The mole ratio of copper sulfate, formaldehyde, and pyridine equals 1:20:1, while the mass ratio of copper sulfate and Ag-MOR is 1:5.0.2 mmol/L EDTA-2Na was dissolved in deionized water as the complexing agent of the reaction, then 0.4 mmol/L copper sulfate solution was added as the main salt to the complexing agent. Sodium hydroxide was added to ensure the pH value of the mixture was above 12.5. The prepared Ag-MOR was added to the mixture in a three-ported flask by stirring under a water heating bath at 70 °C for 2 h, while the ammonia solution was added to ensure the mixture's pH value was consistently higher than 12.5. The mixture was filtered to obtain the filter cake that needed to be washed with deionized water to achieve neutrality. The static Cu/Ag-MOR was synthesized by drying the filter cake in the oven at 110 °C for 24 h.

2.2.3. Preparation of dynamic Cu-MOR

The method of preparing dynamic Cu-MOR is the same as that of dynamic Cu/Ag-MOR; the difference step is that the parallel solution should be added to the mordenite instead of Ag-MOR.

2.3. Characterization of the adsorbents

The powder X-ray diffraction (XRD) patterns of the as-prepared adsorbents were recorded by an X-ray diffractometer (Rigaku Ultima IV, Japan) at a scanning rate of 6°/min for 2θ ranging from 10° to 80°. X-ray photoelectron spectroscopy (XPS) spectrometer (Thermo-Fisher ESCAL-AB^{TM}250Xi, American) was used to analyze the chemical state of elements in the adsorbents by Al Kα radiation as the excitation source. Fourier transform infrared (FT-IR) spectroscopy was carried out on powder samples in the range 400–4000 cm^{-1} using a Fourier transform infrared spectrometer (Nicolet iS 5 F T-IR, American) to obtain the type and amount of functional groups contained on the surface of the sample. The morphologies of the as-prepared adsorbents were characterized by a field emission scanning electron microscopy (SEM, ZEISS Gemini 300, Germany) with an accelerating voltage of 2 kV and a high-resolution transmission electron microscopy (HRTEM, JOEL JEM-2100 F, Japan) with the accelerating voltage of 20 kV. In addition, an energy-dispersive X-ray spectrometer (EDS) was attached with ZEISS Gemini 300 microscopy to determine the element content. The specific surface area, average pore size, and pore volume were determined by Brunauer Emmett Teller (BET) method on a specific surface area aperture analyzer (BUILDER KUBO-X1000, China) by nitrogen adsorption isotherms at 26.85 K.

2.4. Adsorption experiments

The adsorption experiment was to determine the removal rate of the prepared samples; potassium iodide solution was simulated as wastewater. First, 0.083 g potassium iodide was dissolved in a 50 ml volumetric flask with deionized water to obtain 10 mmol/L potassium iodide solution. To obtain 0.5 mmol/L potassium iodide solution, 12.5 ml 10 mmol/L potassium iodide solution was added to a 250 ml volumetric flask with deionized water. Put 100 mg prepared samples into 100 ml 0.5 mmol/L potassium iodide solution, respectively, and stir for 24 h to filter. Next, 1.25 ml filtrate was moved to a 25 ml volumetric flask; the deionized water was added to ensure the volume. The concentration of I^- can be calculated by measuring the adsorbance.

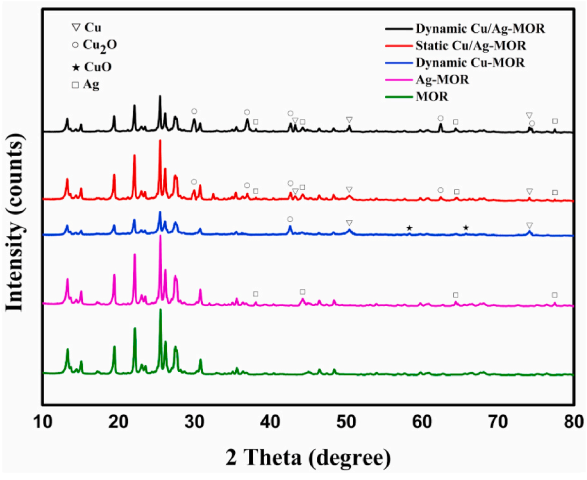

Fig. 1. XRD patterns of Cu/Ag-MOR under different preparation methods.

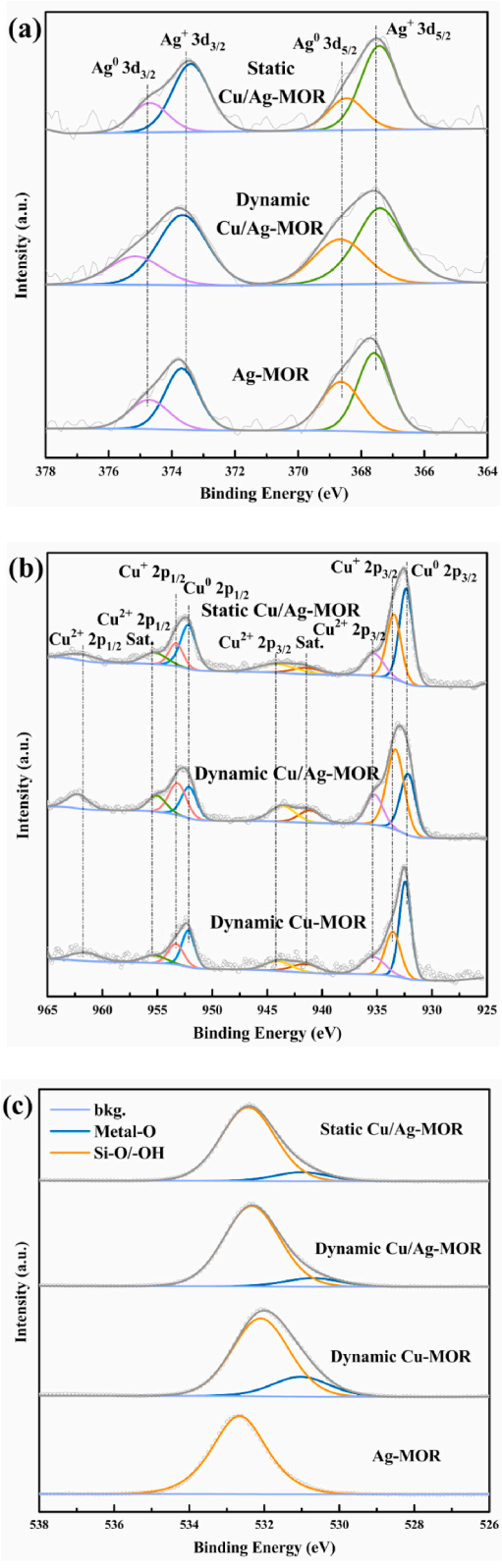

Fig. 2. XPS spectra of (a) Ag 3 d spectra; (b) Cu 2p spectra; (c) O 1s spectra.

3. Results and discussion

3.1. Characterization of the synthesized various adsorbent materials

Fig. 1 showed the phase composition of a series of adsorbents. All the adsorbents contained the characteristic peak of the mordenite molecular sieve. It showed that mordenite has a stable structure and crystal phase, which could not be changed by the metal loading. When the diffraction peaks were at 2θ equaled 38.12°, 44.28°, 64.43°, and 77.47°, (111), (200), (220), and (311) crystal plane could be related to Ag. The peaks attributed to Cu can be found in (111), (200), and (220) were represented at 43.30°, 50.43°, and 74.13°, respectively. Cu_2O of (110), (111), (200), (220), and (311) crystal planes corresponded to 2θ equaled 29.98°, 37.01°, 42.61°, 62.44°, and 74.40°. The diffraction peaks where 2θ equaled 58.34°, 65.79° of CuO in dynamic Cu-MOR indicated the (202), (022) crystal planes. For the dynamic Cu/Ag-MOR, there were Cu_2O, Cu, and Ag species existed, while dynamic Cu-MOR contained CuO, Cu_2O, Cu, and Ag species. Ag could react with CuO to form Ag_2O and Cu_2O, which was proved by the previous study. The addition of Ag enhanced the formation of Cu_2O. It might affect the chemical state and electronic structures of the metal nanoparticles on the MOR surface, which would be further studied by XPS.

XPS analysis was performed to study the chemical state of the elements in the adsorbent, especially the influence of silver on the electronic structure of copper. Fig. 2b showed the XPS spectra of Cu 2p. For dynamic Cu-MOR, there were three peaks at the binding energy of 532.9 eV, 531.6 eV, and 531.4 eV, which were attributed to the oxygen atoms in the mordenite. The Cu–O bonds of CuO and Cu_2O, respectively. With adding Ag, the peak at the binding energy of 532.9 eV was not changed, while oxygen combined with Cu changed. The binding energy of 531.6 eV disappeared, which indicated that CuO reacted with Ag to form Cu_2O totally.

After the Ag particles were induced, the Cu (II) decreased while Cu (I) increased. In contrast with static chemical plating, dynamic chemical plating had a more stable environment for copper species that produced more Cu (I). According to Fig. 2c, physically adsorbed oxygen was shown as *Si*–O or Si–OH without inducing copper species. However, lattice oxygen was produced by inducing copper species. Thus in dynamic Cu/Ag-MOR, lattice oxygen was performed as CuO, which confirmed the previous result.

The XPS analysis was conducted to identify the surface oxidation states of the Ag species on the dynamic Cu/Ag-MOR. Fig. 2a showed that there were two XPS peaks of Ag 3 d, which were at a binding energy of 368.5 ($3d_{5/2}$) and 374.7 eV ($3d_{3/2}$), respectively. It could be assigned to Ag^0, which was consistent with the results of XRD.

This doping of Ag influenced the electronic structure of Cu species loaded on the surface of MOR, which was observed in the XPS spectra. Furthermore, the metal doping would also affect the surface morphology and structure of the adsorbent.

The FTIR spectra of the static Cu/Ag-MOR and dynamic Cu/Ag-MOR samples are shown in Fig. 3. *Si*–*O*–Si symmetric stretching vibration at 814 cm^{-1} and *Si*–O bending vibration at 457 cm^{-1}. The difference was that the static Cu/Ag-MOR sample had possible Cu–O stretching vibrations at 640 cm^{-1} and 560 cm^{-1} and the dynamic Cu/Ag-MOR sample had Cu–O stretching vibrations at 641 cm^{-1} and 564 cm^{-1}, which may be due to the difference in copper species between the two. However, the other peaks in the IR pattern were almost not significantly different, indicating that the two samples contained the same type of functional groups on the surface and the proportional content of functional groups is similar. SEM and HRTEM studies were performed to estimate the effects of Ag on the micromorphology of Cu/Ag-MOR.

Fig. 4 showed the SEM images of the adsorbents prepared with different methods. MOR as the suppory only had the plate-like and rod-like structures (Fig. 4a), and Cu-MOR had the above structure and some particles dispersed on the skeletons (Fig. 4c), which indicated that these particles were copper species with 5.75% of copper bells (Fig. 5b) and poor dispersion. The MOR with high crystallinity had the plate structure with the thickness of 78–90 nm and the width of 440–560 nm. The MOR with low crystallinity had

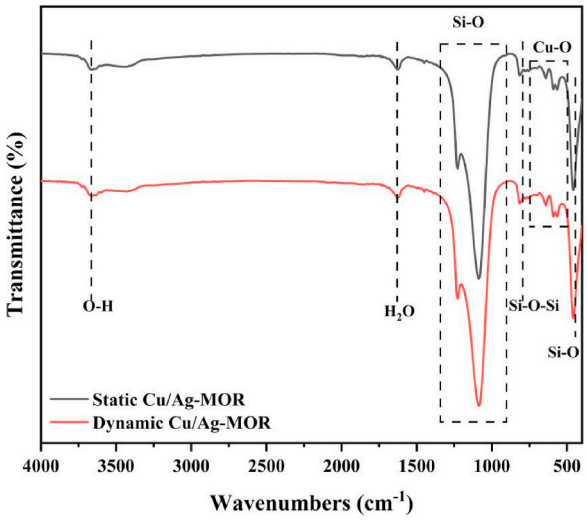

Fig. 3. FTIR spectra of static Cu/Ag-MOR and dynamic Cu/Ag-MOR samples.

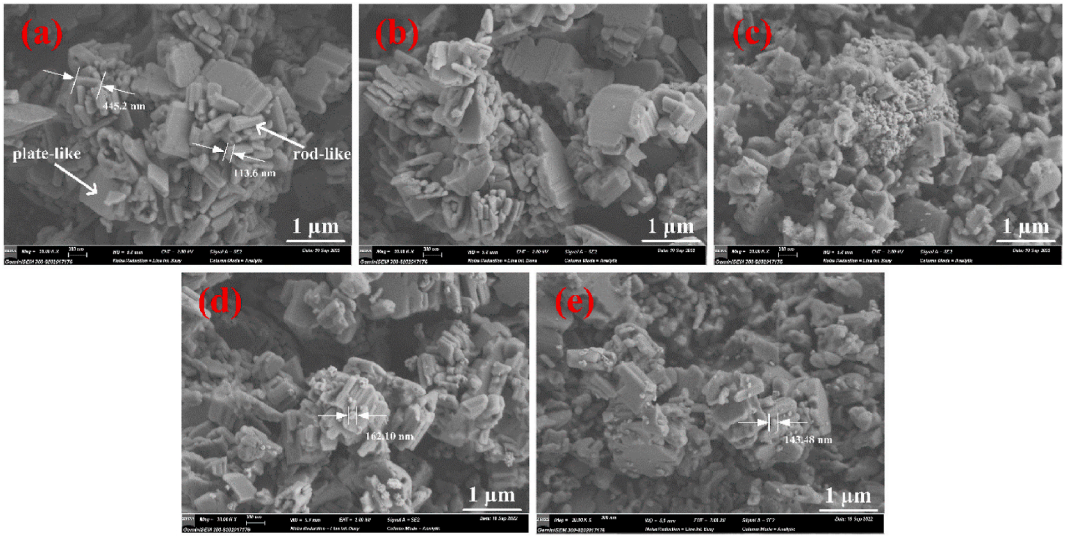

Fig. 4. SEM images of (a) MOR, (b) Ag-MOR, (c) dynamic Cu-MOR, (d) static Cu/Ag-MOR, and (e) dynamic Cu/Ag-MOR.

the rod structure with a length of 0.45 μm and a diameter of 0.11 μm (Fig. 4a).

Figs. 4b and 5a showed Ag-MOR had the similar structure to MOR with a less Ag content, which indicated Ag was evenly distributed in the pore structure and had little effect on the crystallinity of MOR. In contrast, the modification of copper species had an important influence on the crystallinity of MOR. Fig. 4c–e showed the micromorphology of dynamic Cu-MOR, and Cu/Ag-MOR was mainly plate-like structures and some particles dispersed on their surface, which probably was the copper species. Compared with Cu-MOR, Cu/Ag-MOR had the smaller particles and good dispersion. Moreover, the copper particles prepared with dynamic method (Figs. 4e and 125–160 nm) had the smaller sized than that with static method (Figs. 4d and 155–180 nm). Dynamic Cu-MOR contained stacked copper species, while Cu/Ag-MOR contained well-dispersed copper particles. In addition, the dynamic Cu/Ag-MOR had the smaller Cu species than static Cu/Ag-MOR, even though the former contained more copper content (Fig. 5c and d).

Based on the information, these results indicated that silver had a positive effect on the dispersion of copper species, and the dynamic chemical plating method could prepare smaller copper particles by inhibiting their agglomeration, which probably influenced the adsorbability.

In addition to SEM, TEM studies were also performed to estimate the metal distribution on the MOR. Among them, the morphology and pore size of the MOR carrier can be seen in Fig. 6a and b After the loading of the active component Ag, Fig. 6c and d showed that silver particles with the mean size of 9.15 nm were dispersed well in the Ag-MOR, which were in good agreement with the results of SEM. For the TEM images dynamic Cu/Ag-MOR, there were some clusters (7.5–10.2 nm) with good dispersion grow on the MOR (Fig. 6e and f), which were probably assigned to the silver as the core coated by copper species. The $Cu(OH)_4^{2-}$ formed from the combination of $CuSO_4$ and NaOH could be reduced by formaldehyde to generate Cu_2O, which heterogeneously nucleated on Ag particles. The Cu_2O/Ag could be treated as the nucleation sites for subsequent epitaxial growth of copper species domains [34–36]. The silver of Ag-MOR as the nucleation center enhanced the dispersity of copper species. Deposition of copper species, especially cuprous oxide on Ag-MOR would be further studied.

Based on the result of the BET method (Table 1), the pore structure of MOR was not changed by adding Ag particles. Without the Ag particle as the inducing agent, the pore structure of MOR will be expanded and blocked by the overlapped copper species. The overlapping copper species clogged the MOR pores, reducing the specific surface area of the MOR to 6.92 m^2/g and the pore volume from 0.23 cm^2/g to 0.09 cm^2/g. Ag-induced Cu/Ag-MOR material with Cu/Ag loaded onto the MOR backbone as the active center. As a result, the average pore volume and specific area of Cu/Ag-MOR were less than MOR, which was 0.14 cm^2/g and 34–37 m^2/g. According to Fig. 7a, the isothermal curves of the material conform to the Class IV isothermal curve, resulting in a post-delay ring of H_3, which was a slit pore formed by the accumulation of sheet particles. As the comparison of the Barret-Joyner-Halenda (BJH) plots of MOR and dynamic Cu/Ag-MOR shown (Fig. 7b), the pore volumes of 3.5–4.8 nm, 5.1–6.2 nm, 6.6–7.3 nm and more extensive than 10 nm were reduced in MOR, which was caused by the loading of Cu/Ag particles. However, the Cu/Ag intervention did not significantly change the pore size, which proved that the Cu/Ag particles were loaded on the carrier surface, whereas dynamic Cu/Ag-MOR was still a mesoporous material.

3.2. *The deposition rate of Cu_2O in the Ag-MOR*

Based on the results above, NaOH as the precipitant could provide hydroxyl radical to copper ions (II) to generate Cu or Cu_2O with the formaldehyde used as reducing agent. Therefore, pH value might affect composite state of copper and silver. The effects of pH value on the deposition rate of Cu_2O in the Ag-MOR were investigated. Fig. 8 showed the deposit rate of Cu_2O increased with the increasing

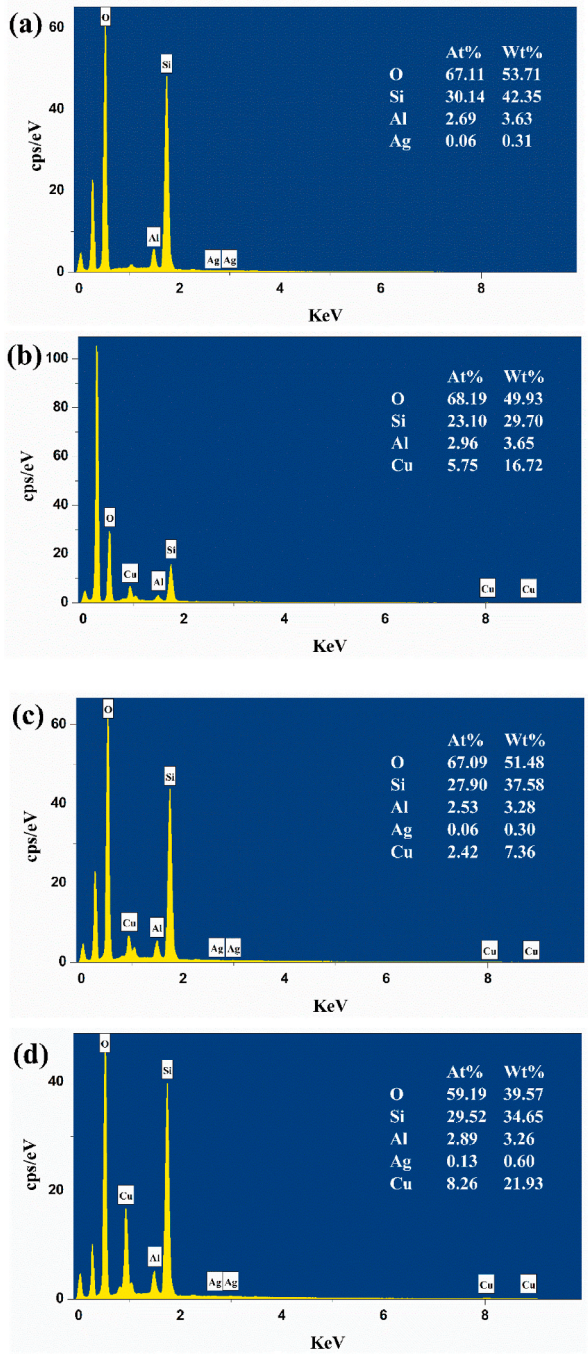

Fig. 5. EDS of (a) Ag-MOR, (b) dynamic Cu-MOR, (c) static Cu/Ag-MOR, and (d) dynamic Cu/Ag-MOR.

of pH ranged from 11 to 12.5. The higher concentration of OH^- could precipitate more copper ions, which was attributed to the increasing deposition rate of $Cu(OH)_4^{2-}$. While too high concentration of OH^- might lead to the decomposition of reducing agent, which decreased the deposition rate of Cu_2O. 12.5 was the best pH value to ensure the rapid precipitation of copper ions.

The effect of EDTA-2Na concentration and pyridine volume on the deposition rate of Cu_2O was also studied. The deposition rate of Cu_2O increased first and then decreased with the increasing concentration of EDTA-2Na. EDTA-2Na could stabilize copper ions by complexing to prevent them from forming too large particles due to too large surface energy. Too much EDTA-2Na in the solution might increase the critical concentration of precipitation of Cu species and then decrease the deposition rate of Cu_2O. As can be seen from Fig. 9, the best concentration of EDTA-2Na was 0.064 mmol L^{-1}.

In addition, the effect of preparation temperature on the deposition rate of Cu_2O was investigated. As shown in Table 2, the

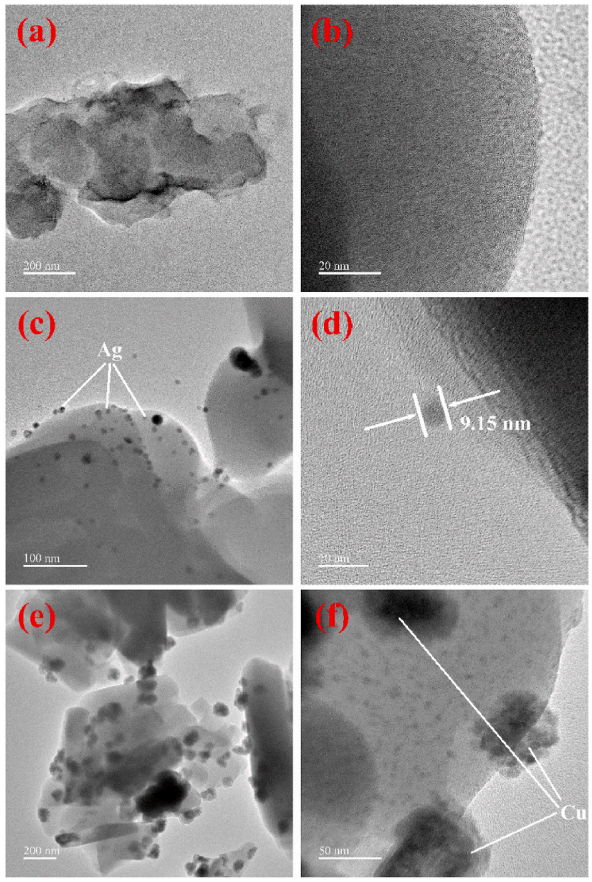

Fig. 6. TEM microphotographs of (a) and (b) MOR, (c) and (d) Ag-MOR, (e) and (f) dynamic Cu/Ag-MOR.

Table 1
BET characterization results of the prepared samples.

Samples	Specific surface area (m^2/g)	Average pore size (nm)	Pore volume (cm^2/g)
MOR	57.83	7.97	0.23
Ag-MOR	42.33	11.02	0.23
Dynamic Cu-MOR	6.92	25.43	0.09
Static Cu/Ag-MOR	34.24	7.96	0.14
Dynamic Cu/Ag-MOR	36.75	6.75	0.14

deposition rate increased with the increasing temperature. The higher the temperature was, the faster the mass transfer rate in the solution was, and the faster the copper coating could be formed. The results showed activation energy of the dynamic Cu_2O deposition rate was 20.31 kJ/mol (Fig. 10), which was lower than the static Cu_2O deposition rate.

The activation energy was calculated by the Arrhenius equation as followed.

$$\mathbf{lnv} = -\frac{\mathbf{E_\alpha}}{\mathbf{RT}} + \mathbf{B} \tag{1}$$

Where v ($mg{\cdot}cm^{-2}{\cdot}h^{-1}$) denoted the Cu_2O deposition rate, E_α was the apparent activation energy, and B was the integration constant. The mole gas constant R was a thermodynamic constant with a value approximately equaled to 8.3145 J/(mol·K). T represented thermodynamic temperature.

3.3. Adsorption performance

The kinetic effects of different adsorbent materials on the adsorption of iodine ions were obtained by fitting. As shown in Fig. 11, the physical adsorption rate could reach 52% when MOR was set as the adsorbent. When Ag-MOR and Cu/Ag-MOR were set as the adsorbent, the adsorption efficiency increased with time, which overgrew for the first 20 min but slowed down between 20 and 70 min.

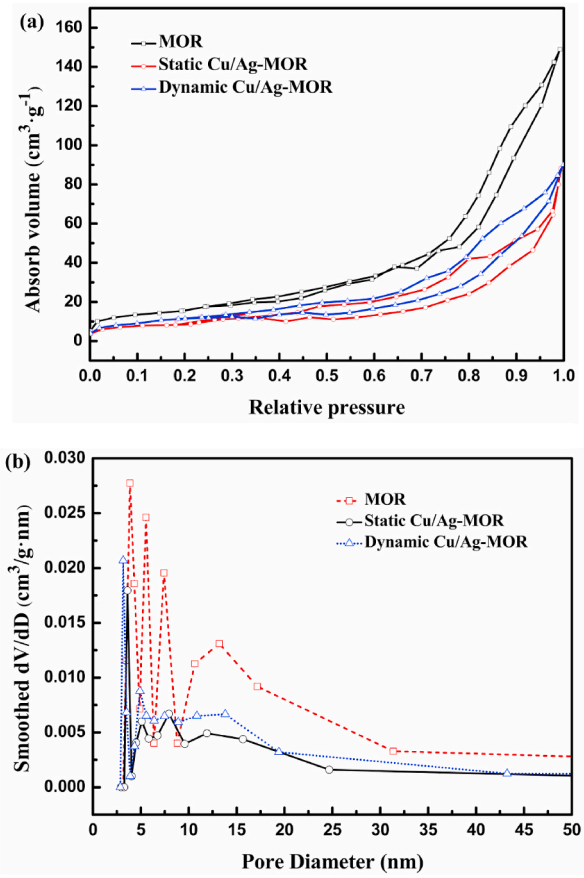

Fig. 7. (A) N2 adsorption-desorption isotherms of MOR, static Cu/Ag-MOR, and dynamic Cu/Ag-MOR. (b) BJH adsorption pore size distribution of MOR, static Cu/Ag-MOR, and dynamic Cu/Ag- MOR.

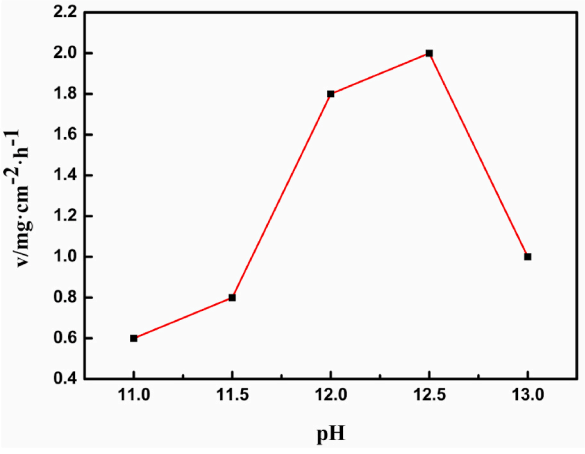

Fig. 8. The plot of Cu_2O deposition rate versus pH.

After 70 min, the capture material reached saturation. While dynamic Cu/Ag-MOR materials can reached 99.1% saturation adsorption efficiency.

According to the line dynamic Cu/Ag-MOR in Fig. 11, from 0 to 20 min, the copper species were distributed uniformly by inducing Ag particles. Moreover, there were more adsorption active sites in Cu/Ag-MOR, which improved the adsorption rate. At 20–70 min, CuI was produced by copper species that adsorb iodine ions in the curing solution. After 70 min, the chemisorption ended; the Cu/Ag-

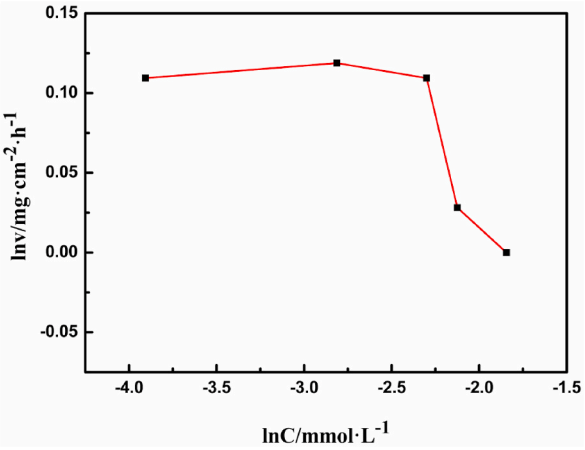

Fig. 9. Plot of Cu_2O deposition rate versus EDTA-2Na concentration.

Table 2
Cu_2O deposition rate as a function of temperature.

T/°C	35	40	45	50	55	60	65	70	75
Dynamic Cu/Ag-MOR of v	1.010	1.018	1.026	1.035	1.043	1.054	1.062	1.070	1.071
Static Cu/Ag-MOR of v	1.007	1.020	1.035	1.055	1.067	1.083	1.097	1.112	1.115

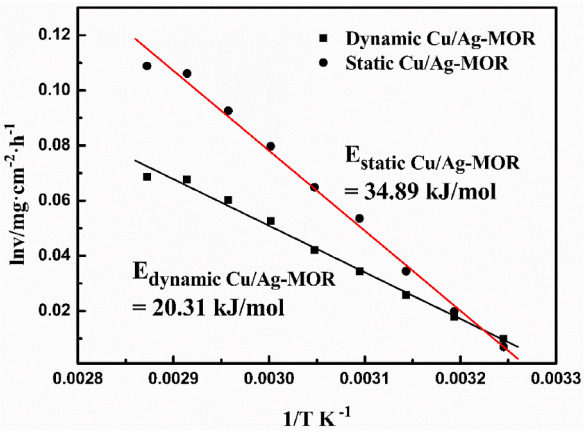

Fig. 10. Plot of the logarithm of Cu_2O deposition rate versus the inverse of temperature.

MOR material reached its critical capacity while the adsorption reached saturation.

Fig. 12 was fitted by the secondary reaction rate equation, which is:

$$\frac{dq_t}{dt} = K_2(q_m - q_t)^2 \tag{2}$$

Where q_t (mmol·g^{-1}) denoted the adsorption capacity at time t (min), K_2 represented the fitted second-order rate constant that equaled 6.080, and q_m meant average adsorption capacity that equaled 0.050 mmol g^{-1}.

Integrated the above equation by substituting the boundary conditions of $t = 0$ and $q_t = 0$, the equation can be simplified as:

$$\frac{1}{(q_m - q_t)} = \frac{1}{q_m} + K_2 t \tag{3}$$

The linear pseudo-second-order model can be obtained by rearranging and combining the equations, and its mathematical expression is:

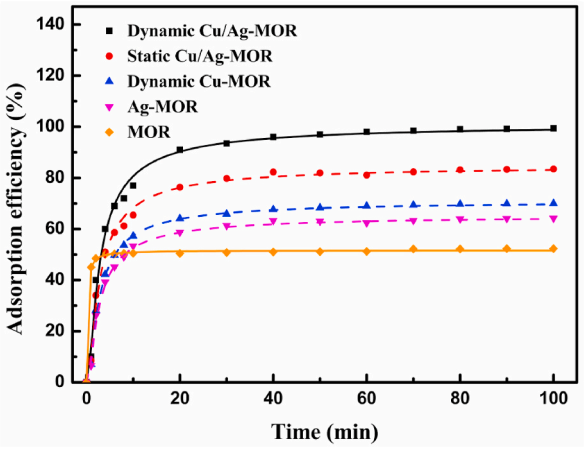

Fig. 11. Adsorption performance of I^- adsorption by various adsorbent materials.

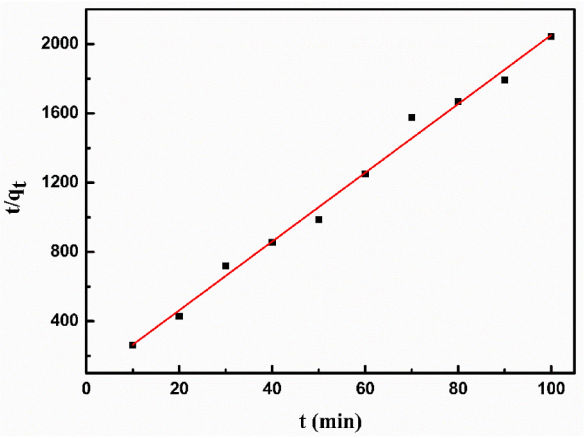

Fig. 12. A pseudo-second-order plot of linearity of captured iodide ions t/q_t versus time t.

$$\frac{t}{q_t} = \frac{1}{K_2 q_m^2} + \frac{1}{q_m} t \tag{4}$$

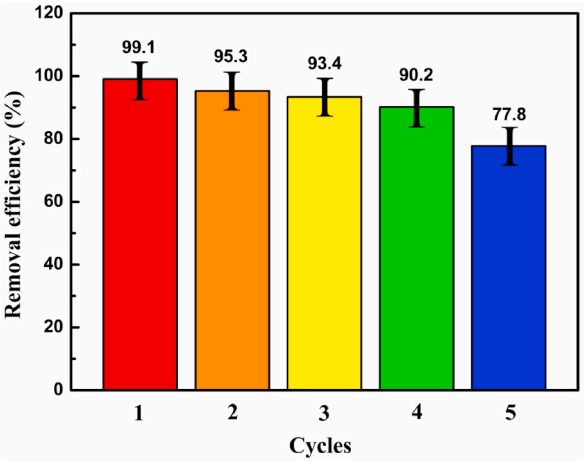

Fig. 13. Reusability of dynamic Cu/Ag-MOR nanoadsorbent for the adsorption/desorption of I^-.

The linear equation ($t/q_t = 19.8533t+65.7857$) can be obtained by plotting t/q_t versus time, while the linear regression coefficient (R^2) of the fitted curve of this kinetic equation is 0.9957. Thus, it indicated that the fitted adsorption reaction model could predict the kinetic behavior of the adsorption reaction.

3.4. Desorption and reusability study

The reusability of the dynamic Cu/Ag-MOR nano adsorbent was evaluated over five successive cycles in adsorption-desorption experiments. The reusability results are shown in Fig. 13. After four consecutive adsorption-desorption cycles, in total, the removal of I^- decreased by 8.9%. In the fifth successive adsorption-desorption cycle, the adsorption rate of I^- decreased to 77.8%, a decrease of 21.3%. Dynamic Cu/Ag-MOR exhibited good regeneration performance, and thus it may be reused as an efficient nanoadsorbent.

3.5. Effect of miscellaneous contaminant samples

To study the effect of the intervention of miscellaneous contaminants on the adsorption of I^- by the material, the same molar amounts of competing anions Cl^-, CO_3^{2-}, SO_4^{2-} and NO_3^- were added to a solution of I^- at an initial concentration of 0.5 mmol/L. Dynamic Cu/Ag-MOR was used as the adsorbent material for the I^- adsorption tests. As shown in Fig. 14, the adsorption efficiencies of iodide ions were 99.1%, 97.6%, 99.3% and 98.8% in the presence of Cl^-, CO_3^{2-}, SO_4^{2-} and NO_3^- in solution, respectively. The results showed that the presence of anions such as Cl^-, CO_3^{2-}, SO_4^{2-} and NO_3^- did not affect the iodine adsorption capacity of the dynamic Cu/Ag-MOR material. This demonstrates that the dynamic Cu/Ag-MOR material shows good applicability in complex situations where miscellaneous contaminants co-exist.

4. Conclusions

In summary, this study's preparation method of Cu/Ag-MOR is simple and easy to control in the experiment condition. The dopping of Ag particles could enhance the selectivity of Cu (I), which produced better Cu (I) crystalline composites in the stable dynamic system. Dynamic Cu/Ag-MOR have uniform mesoporous structure, which could effectively adsorb small diameter molecules into the interior of the pore cavity. Also, it has a good adsorption effect on iodine ions through controlled chemisorption combined with physical adsorption. Within 70 min, dynamic Cu/Ag-MOR material could achieve the best adsorption effect, which reached a 99.1% rate of removal of iodine ions. In addition, dynamic Cu/Ag-MOR materials have good regenerative properties and can be recycled many times. Dynamic Cu/Ag-MOR materials show good suitability in complex situations where miscellaneous contaminants co-exist. The adsorption mechanism of Cu (I) adsorption of iodine ions was proposed, and the adsorption kinetic fitting proved that chemisorption was the control step of the adsorption process. Therefore, dynamic Cu/Ag-MOR could be used as an excellent capture material that adsorbs the radioactive iodine ions. Also, this material will help reduce pollution and protect the environment, which better contributes to the sustainable development of human beings. As the adsorption capacity of the adsorbent material was sufficiently high, the disposal and reuse of the recovered material was not considered in the study.

Author contribution statement

Guowei Yuan: Conceived and designed the experiments; Performed the experiments; Analyzed and interpreted the data; Contributed reagents, materials, analysis tools or data; Wrote the paper.

Yizhong Lu: Contributed reagents, materials, analysis tools or data.

Cheng Yang: Analyzed and interpreted the data; Contributed reagents, materials, analysis tools or data.

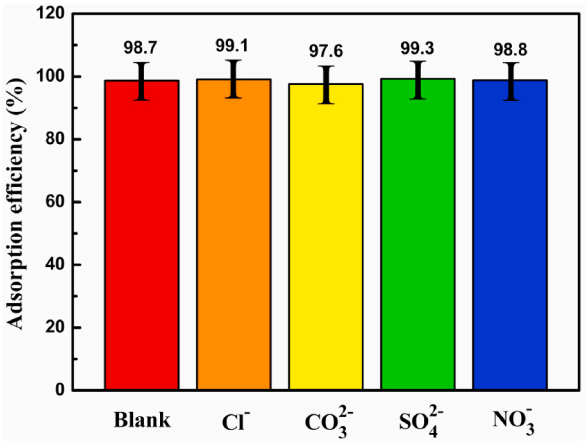

Fig. 14. Effect of high concentrations of Cl^-, CO_3^{2-}, SO_4^{2-} and NO_3^- on the adsorption of I^- anions by dynamic Cu/Ag-MOR.

Data availability statement

Data will be made available on request.

Declaration of competing interest

The authors declare that they have no known competing financial interests or personal relationships that could have appeared to influence the work reported in this paper.

Acknowledgments

The authors acknowledge the financial support from the National Natural Science Foundation of China (21705056) and the Key R&D Program of Shandong Province (2019GSF111068).

References

[1] R. Rohde, R. Muller, Air pollution in China: mapping of concentrations and sources, PLoS One 10 (8) (2015), e0135749, https://doi.org/10.1371/journal.pone.0135749.
[2] G. Wong, L. Zhang, Geochemical dynamics of iodine in marginal seas: the southern East China Sea, Deep Sea Res. Part II Top. Stud. Oceanogr. 50 (6–7) (2003) 1147–1162, https://doi.org/10.1016/s0967-0645(03)00015-8.
[3] L. Liu, W. Liu, X. Zhao, et al., Selective capture of iodide from solutions by microrosette-like δ-Bi_2O_3, ACS Appl. Mater. Interfaces 6 (18) (2014) 16082–16090, https://doi.org/10.1021/am504000n.
[4] T. Zhang, G. Yin, C. Wang, et al., Engineering mesoporous algal-based biochars for efficient remediation of norfloxacin pollution in marine environment, Environ. Adv. 9 (2022), 100302, https://doi.org/10.1016/j.envadv.2022.100302.
[5] V. Hansen, P. Yi, X. Hou, et al., Iodide and iodate (^{129}I and ^{127}I) in surface water of the baltic sea, kattegat and skagerrak, Sci. Total Environ. 412–413 (2011) 296–303, https://doi.org/10.1016/j.scitotenv.2011.10.001.
[6] X. Hou, P.P. Povinec, L. Zhang, et al., Iodine-129 in seawater offshore fukushima: distribution, inorganic speciation, sources, and budget, Environ. Sci. Technol. 47 (7) (2013) 3091–3098, https://doi.org/10.1021/es304460k.
[7] D. Yang, H. Liu, L. Liu, et al., Silver oxide nanocrystals anchored on titanate nanotubes and nanofibers: promising candidates for entrapment of radioactive iodine anions, Nanoscale 5 (22) (2013), 11011, https://doi.org/10.1039/c3nr02412a.
[8] S. Sun, X. Sha, J. Liang, et al., Rapid synthesis of polyimidazole functionalized Mxene via microwave-irradiation assisted multi-component reaction and its iodine adsorption performance, J. Hazard Mater. 420 (2021) 126580–126590, https://doi.org/10.1016/j.jhazmat.2021.126580.
[9] X. Li, D. Zeng, Z. He, et al., Magnetic chitosan microspheres: an efficient and recyclable adsorbent for the removal of iodide from simulated nuclear wastewater, Carbohydrate Polym. 276 (2022) 118729–118739, https://doi.org/10.1016/j.carbpol.2021.118729.
[10] F.L. Theiss, S.J. Couperthwaite, G.A. Ayoko, et al., A review of the removal of anions and oxyanions of the halogen elements from aqueous solution by layered double hydroxides, J. Colloid Interface Sci. 417 (2014) 356–368, https://doi.org/10.1016/j.jcis.2013.11.040.
[11] F. Li, X. Zhang, X. Zhao, Influence of ion exchange resin on the performance of continuous electrodeionization (CEDI) treating low-level radioactive wastewater, J. Nucl. Sci. Technol. 54 (12) (2017) 1355–1360, https://doi.org/10.1080/00223131.2017.1366877.
[12] M.M. Hamed, M. Holiel, Y.F. El-Aryan, Removal of selenium and iodine radionuclides from waste solutions using synthetic inorganic ion exchanger, J. Mol. Liq. 242 (2017) 722–731, https://doi.org/10.1016/j.molliq.2017.07.035.
[13] L. Ding, Y. Wei, Y. Wang, et al., A two-dimensional lamellar membrane: MXene Nanosheet Stacks, Angew. Chem. Int. Ed. 56 (7) (2017) 1825–1829, https://doi.org/10.1002/anie.201609306.
[14] Q. Huang, M. Liu, L. Mao, et al., Surface functionalized SiO_2 nanoparticles with cationic polymers via the combination of mussel inspired chemistry and surface initiated atom transfer radical polymerization: characterization and enhanced removal of organic dye, J. Colloid Interface Sci. 499 (2017) 170–179, https://doi.org/10.1016/j.jcis.2017.03.102.
[15] S.D. Balsley, P.V. Brady, J.L. Krumhansl, et al., Iodide retention by metal sulfide surfaces: cinnabar and chalcocite, Environ. Sci. Technol. 30 (10) (1996) 3025–3027, https://doi.org/10.1021/es960083c.
[16] D. Yang, S. Sarina, H. Zhu, et al., Capture of radioactive cesium and iodide ions from water by using titanate nanofibers and nanotubes, Angew. Chem. 123 (45) (2011) 10782–10786, https://doi.org/10.1002/ange.201103286.
[17] L. Zhang, X. Wang, Photocatalytic performance of Cu_2O and Ag/Cu_2O composite octahedra prepared by a propanetriol-reduced process, Appl. Phys. A 117 (4) (2014) 2189–2196, https://doi.org/10.1007/s00339-014-8644-4.
[18] P. Mao, Y. Liu, X. Liu, et al., Bimetallic AgCu/Cu_2O hybrid for the synergetic adsorption of iodide from solution, Chemosphere 180 (2017) 317–325, https://doi.org/10.1016/j.chemosphere.2017.04.038.
[19] S. Liu, N. Wang, Y. Zhang, et al., Efficient removal of radioactive iodide ions from water by three-dimensional Ag_2O-Ag/TiO_2 composites under visible light irradiation, J. Hazard Mater. 284 (2015) 171–181, https://doi.org/10.1016/j.jhazmat.2014.10.054.
[20] P. Mao, B. Qi, Y. Liu, et al., Ag^{II} doped MIL-101 and its adsorption of iodine with high speed in solution, J. Solid State Chem. 237 (2016) 274–283, https://doi.org/10.1016/j.jssc.2016.02.030.
[21] G. Lefèvre, A. Walcarius, J. Ehrhardt, et al., Sorption of iodide on cuprite (Cu_2O), Langmuir 16 (10) (2000) 4519–4527, https://doi.org/10.1021/la9903999.
[22] M. Zhao, S. Wang, H. Wang, et al., Application of sodium titanate nanofibers as constructed wetland fillers for efficient removal of heavy metal ions from wastewater, Environ. Pollut. 248 (2019) 938–946, https://doi.org/10.1016/j.envpol.2019.02.040.
[23] X. Zhao, X. Yu, X. Wang, et al., Recent advances in metal-organic frameworks for the removal of heavy metal oxoanions from water, Chem. Eng. J. 407 (2021), 127221, https://doi.org/10.1016/j.cej.2020.127221.
[24] Y. Guo, H. Zhang, N. Tao, et al., Adsorption of malachite green and iodine on rice husk-based porous carbon, Mater. Chem. Phys. 82 (1) (2003) 107–115, https://doi.org/10.1016/s0254-0584(03)00191-3.
[25] Y. Wang, G.A. Sotzing, R.A. Weiss, Sorption of iodine by polyurethane and melamine-formaldehyde foams using iodine sublimation and iodine solutions, Polymer 47 (8) (2006) 2728–2740, https://doi.org/10.1016/j.polymer.2006.02.063.
[26] V.P. Kothavale, A. Sharma, R.P. Dhavale, et al., Hyperbranched amino modified magnetic nanoparticles for simultaneous removal of heavy metal ions from aqueous solutions, Mater. Chem. Phys. (2022) 292, https://doi.org/10.1016/j.matchemphys.2022.126792.
[27] P.P. Bote, S.R. Vaze, C.S. Patil, et al., Reutilization of Carbon from Exhausted Water Filter Cartridges (EWFC) for Decontamination of Water: an Innovative Waste Management Approach, 24, Environmental Technology & Innovation, 2021, https://doi.org/10.1016/j.eti.2021.102047.
[28] V.P. Kothavale, A. Sharma, R.P. Dhavale, et al., Carboxyl and thiol-functionalized magnetic nanoadsorbents for efficient and simultaneous removal of Pb(II), Cd (II), and Ni(II) heavy metal ions from aqueous solutions: studies of adsorption, kinetics, and isotherms, J. Phys. Chem. Solid. 172 (2023), https://doi.org/10.1016/j.jpcs.2022.111089.
[29] K. Yoshinori, E. Yuki, I. Yasunori, et al., Hydrogen and water vapor adsorption properties on cation-exchanged mordenite for use to a tritium recovery system, Fusion Eng. Des. 89 (7–8) (2014) 1539–1543, https://doi.org/10.1016/j.fusengdes.2014.01.064.

[30] A. Ananthanarayanan, S.A. Khot, V. Jaiswal, et al., Effect of NO_x on AgI formation in Ag-mordenite, Int. J. Environ. Stud. 74 (2) (2017) 192–201, https://doi.org/10.1080/00207233.2017.1280317.
[31] Q. Lu, W. Qian, H. Ma, et al., Silver-modified nano mordenite for carbonylation of dimethyl ether, Catalysts 11 (2021) 197, https://doi.org/10.3390/catal11020197.
[32] P. Mao, Y. Liu, Y. Jiao, et al., Enhanced uptake of iodide on Ag@Cu_2O nanoparticles, Chemosphere 164 (2016) 396–403, https://doi.org/10.1016/j.chemosphere.2016.08.116.
[33] P. Mao, L. Qi, X. Liu, et al., Synthesis of Cu/Cu_2O hydrides for enhanced removal of iodide from water, J. Hazard Mater. 328 (2017) 21–28, https://doi.org/10.1016/j.jhazmat.2016.12.065.
[34] J. Seon, Y. Hwang, Cu/Cu_2O-immobilized cellulosic filter for enhanced iodide removal from water, J. Hazard Mater. 409 (2021), 124415, https://doi.org/10.1016/j.jhazmat.2020.124415.
[35] T.Y. Kim, M.H. Lee, J. Byun, et al., Influence of reducing agent on chemical decomposition of bis (3-sulfopropyl) disulfide (SPS) in Cu plating bath, J. Electrochem. Soc. 168 (2021) 3, https://doi.org/10.1149/1945-7111/abe727.
[36] S. Tao, M. Yang, H. Chen, et al., Microfluidic synthesis of Ag@Cu_2O core-shell nanoparticles with enhanced photocatalytic activity, J. Colloid Interface Sci. 486 (2017) 16–26, https://doi.org/10.1016/j.jcis.2016.09.051.